Direct and Reversible Hydrogenation of CO_2 to Formate by a Bacterial Carbon Dioxide Reductase

K. Schuchmann and V. Müller

Science **342**, 1382 (2013);
DOI: 10.1126/science.1244758

Science (print ISSN 0036-8075; online ISSN 1095-9203) is published weekly, except the last week in December, by the American Association for the Advancement of Science, 1200 New York Avenue NW, Washington, DC 20005.

whereas typical I_{MiCa} was seen after EMRE re-expression (Fig. 3F) (*6*).

Consistent with EMRE being a core component of the uniplex, when EMRE was lost, the size of the complex on a native gel was reduced to ~300 kD, similar to that in cells lacking MICU1 (Fig. 4A). The observation that loss of either EMRE or MICU1 reduced the size of the native complex to a similar extent raised the hypothesis that EMRE may mediate interaction between MCU and MICU1 and MICU2. To test this, we stably expressed MCU-FLAG, or a control protein in HEK-293T, or HeLa wild-type cells, or cells lacking EMRE and performed FLAG immunoprecipitations. In wild-type cells, MICU1 and MICU2 immunoprecipitated with MCU-FLAG but not with control SDHB-FLAG (Fig. 4B and fig. S4). However, in cells lacking EMRE, the interaction between MCU-FLAG and MICU1 and MICU2 was completely lost (Fig. 4B and fig. S4). Similarly, MCU was not associated with immunoprecipitated MICU1-FLAG in cells lacking EMRE (Fig. 4C). In the absence of EMRE, MCU still oligomerized (Fig. 4, A and B) and interacted with MCUb. Moreover, in the absence of EMRE, the interaction between MICU1 and MICU2 was intact (Fig. 4C). These data indicate that loss of EMRE specifically interrupted the association of MCU with MICU1 and MICU2. Furthermore, MCUb, MICU1, and MICU2 appear to be dispensable for MCU-EMRE interaction because in cells lacking MCUb or MICU1, EMRE was still associated with immunoprecipitated MCU-FLAG (Fig. 4, D and E).

We propose a model in which EMRE interacts with MICU1 and MICU2 in the IMS and with MCU oligomers in the inner membrane, thus linking the calcium-sensing activity of MICU1 and MICU2 to the channel activity of MCU (Fig. 4F). The fact that our immunoprecipitated complex migrates at the same apparent molecular size as the uniporter from purified mitochondria (Fig. 1A), and recovers the founding members of the complex, suggests that we immunoprecipitated all of its components. It is notable that although other proteins have been reported to participate in mitochondrial calcium handling—such as LETM1, NCLX, UCP2 and 3, MCUR1, and TRPC3—they were not recovered in our proteomic assay, suggesting that they play key roles outside of the uniplex. A key insight from the current work is that EMRE is essential for in vivo uniporter current (I_{MiCa}) and that MCU oligomers alone are not sufficient for in vivo uniporter activity, in contrast to what has been suggested using in vitro bilayer studies (*4*). Why MCU needs association with EMRE for in vivo calcium conductance requires further investigation. Phylogenetic analyses indicate that the uniporter must have been a feature of the earliest mitochondria because MCU and MICU1 are found within all major eukaryotic taxa, with lineage-specific losses (*20*). EMRE is unique among human uniplex components in that it appears to have emerged more recently and represents a metazoan innovation. Its identification should help us understand how the activity and regulation of this ancient channel evolved.

References and Notes

1. Y. Kirichok, G. Krapivinsky, D. E. Clapham, *Nature* **427**, 360–364 (2004).
2. F. Perocchi *et al.*, *Nature* **467**, 291–296 (2010).
3. J. M. Baughman *et al.*, *Nature* **476**, 341–345 (2011).
4. D. De Stefani, A. Raffaello, E. Teardo, I. Szabò, R. Rizzuto, *Nature* **476**, 336–340 (2011).
5. M. Plovanich *et al.*, *PLOS ONE* **8**, e55785 (2013).
6. D. Chaudhuri, Y. Sancak, V. K. Mootha, D. E. Clapham, *eLife* **2**, e00704 (2013).
7. J. D. Martell *et al.*, *Nat. Biotechnol.* **30**, 1143–1148 (2012).
8. K. Mallilankaraman *et al.*, *Cell* **151**, 630–644 (2012).
9. G. Csordás *et al.*, *Cell Metab.* **17**, 976–987 (2013).
10. R. Palty *et al.*, *J. Biol. Chem.* **279**, 25234–25240 (2004).
11. D. Jiang, L. Zhao, D. E. Clapham, *Science* **326**, 144–147 (2009).
12. K. Mallilankaraman *et al.*, *Nat. Cell Biol.* **14**, 1336–1343 (2012).
13. S. Feng *et al.*, *Proc. Natl. Acad. Sci. U.S.A.* **110**, 11011–11016 (2013).
14. M. Trenker, R. Malli, I. Fertschai, S. Levak-Frank, W. F. Graier, *Nat. Cell Biol.* **9**, 445–452 (2007).
15. S. E. Ong *et al.*, *Mol. Cell. Proteomics* **1**, 376–386 (2002).
16. A. Raffaello *et al.*, *EMBO J.* **32**, 2362–2376 (2013).
17. A. Krogh, B. Larsson, G. von Heijne, E. L. Sonnhammer, *J. Mol. Biol.* **305**, 567–580 (2001).
18. M. G. Claros, P. Vincens, *Eur. J. Biochem.* **241**, 779–786 (1996).
19. D. J. Pagliarini *et al.*, *Cell* **134**, 112–123 (2008).
20. A. G. Bick, S. E. Calvo, V. K. Mootha, *Science* **336**, 886 (2012).

Acknowledgments: We thank Z. Grabarek and D. M. Shechner for helpful discussions. Y.S. received support from the Helen Hay Whitney Foundation. D.C. received support from NIH F32HL107021. D.E.C. is an Investigator of the Howard Hughes Medical Institute. This work was supported by grants to V.K.M from NIH DK080261 and a gift from W. Dan and Pat Wright.

Supplementary Materials

www.sciencemag.org/content/342/6164/1379/suppl/DC1
Materials and Methods
Figs. S1 to S4
Table S1
References (*21*–*33*)

10 July 2013; accepted 5 November 2013
Published online 14 November 2013;
10.1126/science.1242993

Direct and Reversible Hydrogenation of CO_2 to Formate by a Bacterial Carbon Dioxide Reductase

K. Schuchmann and V. Müller*

Storage and transportation of hydrogen is a major obstacle for its use as a fuel. An increasingly considered alternative for the direct handling of hydrogen is to use carbon dioxide (CO_2) as an intermediate storage material. However, CO_2 is thermodynamically stable, and developed chemical catalysts often require high temperatures, pressures, and/or additives for high catalytic rates. Here, we present the discovery of a bacterial hydrogen-dependent carbon dioxide reductase from *Acetobacterium woodii* directly catalyzing the hydrogenation of CO_2. We also demonstrate a whole-cell system able to produce formate as the sole end product from dihydrogen (H_2) and CO_2 as well as syngas. This discovery opens biotechnological alternatives for efficient CO_2 hydrogenation either by using the isolated enzyme or by employing whole-cell catalysis.

Future energy demands require alternatives for the current energy technologies that are based mainly on fossil fuels. Hydrogen is a promising and widely considered option as alternative energy feedstock, but research on direct hydrogen storage and transportation has not revealed economically usable possibilities (*1*). A promising alternative is the use of CO_2 as storage material for hydrogen (*2*). The near-equilibrium hydrogenation of CO_2 leads to formic acid and the corresponding base formate, respectively. This low energy demand is beneficial for a hydrogen storage application for a hydrogen-using fuel cell. An alternative would be the use of a fuel cell directly using formate (*3*). Unfortunately, high temperatures and pressures are often required for efficient chemical hydrogenation of CO_2 (*4*). Recently, progress has been made by using an iridium catalyst to reversibly hydrogenate CO_2 at near-ambient conditions, but still with moderate catalytic rates (*5*), or by the use of a cobalt-based catalyst in combination with high concentration of an expensive base (*6*).

Biological systems are often promising alternatives for chemically difficult conversions. Even though the reduction of CO_2 is a widely distributed reaction in nature, little is known about enzymes catalyzing CO_2 reduction activity, and no enzyme is known to catalyze the direct hydrogenation of CO_2 alone (*7*, *8*). One isolated formate dehydrogenase (FDH) could be shown to reduce CO_2 electrochemically, but not with H_2 as the electron donor (*9*). Acetogenic bacteria are

Molecular Microbiology and Bioenergetics, Institute of Molecular Biosciences, Johann Wolfgang Goethe University Frankfurt/Main, Max-von-Laue-Strasse 9, 60438 Frankfurt, Germany

*Corresponding author. E-mail: vmueller@bio.uni-frankfurt.de

promising candidates for such enzymes based on the physiological use of H_2 + CO_2 as the sole growth substrate and the production of formate as intermediate (*10*, *11*). One enzyme was reported that can catalyze the hydrogenation of CO_2 at the purified state, but it also uses the reduced form of nicotinamide adenine dinucleotide phosphate (NADPH) and reduced ferredoxin as electron donors in an electron-bifurcating manner (*12*).

Here, we report the discovery of a bacterial hydrogen-dependent carbon dioxide reductase (HDCR) that directly uses dihydrogen for the interconversion of CO_2 to formate from the acetogenic bacterium *Acetobacterium woodii*. We targeted this bacterium because it grows with H_2 + CO_2 at ambient conditions using an ancient pathway for energy conservation. It lives under extreme energy limitation, and a direct use of H_2 for CO_2 reduction would be beneficial for the cell. Moreover, an HDCR was predicted from the genome sequence (*13*).

The HDCR enzyme was purified from cells of *A. woodii* under anaerobic conditions (*14*). The purified protein complex is composed of four different subunits (fig. S1A). It eluted as a single peak from a gel filtration with an apparent mass around 3500 kD but dissociated during separation by clear native page (fig. S2). The calculated molecular mass of the monomeric complex is 169 kD. Peptide mass fingerprinting identified four proteins encoded by the gene cluster *Awo_c08190-08260* (fig. S1, B and C). A putative formate dehydrogenase (FdhF1/2) and an iron-iron hydrogenase (HydA2) form the two large subunits accompanied by two small electron transfer subunits (HycB1/2/3). The genome encodes a selenium-containing (FdhF2) and a selenium-free (FdhF1) FDH whose genes are in tandem on the chromosome. Because cells were grown in selenium-containing media, mostly FdhF2 was found. A gene encoding an electron transfer protein follows each FDH gene. The metal content determined by inductively coupled plasma mass spectrometry (ICP-MS) measurements was 0.6 molybdenum, no tungsten, 0.8 selenium, 0.7 zinc and 39 ± 6 iron atoms. These values are in agreement with the predicted cofactors (table S1).

By using the artificial electron acceptor methylviologen, we were able to measure hydrogenase and FDH activity separately. The isolated enzyme catalyzed formate oxidation with an activity of ~600 μmol formate min^{-1} mg^{-1} and hydrogen oxidation with 10,800 μmol H_2 min^{-1} mg^{-1}. Specific activities varied between different enzyme preparations due to the high oxygen sensitivity. The Michaelis constant (K_M) values for formate and hydrogen were determined to be 1 ± 0.3 mM (SEM; N = 2 independent experiments) and 125 ± 31 μM (SEM; N = 3 independent experiments), respectively (fig. S3). The pH range for maximal activity was between 7 and 9 for both activities (fig. S4). The temperature optimum for hydrogen oxidation was 30°C, that for formate oxidation 40°C (fig. S5). HCO_3^- reductase activity with reduced methylviologen as electron donor was catalyzed with 132 U/mg and a K_M of 37 ± 4 mM HCO_3^- (SEM; N = 3 independent experiments) (fig. S6).

Searching for an enzyme that directly hydrogenates CO_2, we investigated whether the purified complex can catalyze this reaction. The enzyme indeed catalyzed the hydrogenation of CO_2 with a rate of 10 μmol formate produced min^{-1} mg^{-1} (Fig. 1A). Recently reported chemical catalysts promote the hydrogenation of CO_2 at comparable conditions with an initial turnover frequency (TOF) of ~70 $hours^{-1}$ (*5*). The purified HDCR catalyzes the same reaction at 30°C with a TOF of 101,600 $hours^{-1}$. Thus, the enzyme is nearly 1500 times as effective as these chemical catalysts. The reverse reaction, formate oxidation to H_2 and CO_2, was catalyzed with 14 U/mg (Fig. 1B). The enzyme has two advantages in industrial applications. First, it does not need an external cofactor as electron carrier. Cofactor-dependent conversion would raise the cost of such a process even if regeneration systems would be used. Second, the reaction is reversible, and thus the directionality is easy to control by substrate concentrations.

Purified HDCR also catalyzed the reduction of CO_2 with reduced ferredoxin instead of H_2 as electron donor. The rate of ferredoxin-dependent formate production was 0.6 μmol formate min^{-1} mg^{-1} (Fig. 1C). Ferredoxin was reduced by CO dehydrogenase (CODH) from *A. woodii*, leading to formate production from CO. The reverse reaction was catalyzed with rates of 0.6 μmol ferredoxin min^{-1} mg^{-1} and a K_M for ferredoxin of 13 ± 5 μM (SEM; N = 3 independent experiments) (fig. S7). Industrially produced hydrogen often contains remaining CO that is a potent inhibitor of fuel-cell catalysts. Considering *A. woodii* HDCR as a catalyst for hydrogen storage, the side activity represents a possible industrial advantage. Using a combination of HDCR and CODH would allow the complete conversion of gas mixtures containing H_2, CO_2, and CO (Fig. 2).

To get insights into the reaction mechanism of the HDCR, we searched for compounds that inhibit partial reactions. CO turned out to be a potent inhibitor of the hydrogenase activity alone (fig. S8A). In the presence of 10% CO in the gas phase, only the FDH module is active. Under these conditions, formate-dependent ferredoxin reduction rates increased, showing that the hydrogenase moiety is not involved in this electron transfer (fig. S8B). Ferredoxin reduction with rates of 0.4 μmol ferredoxin min^{-1} mg^{-1} was also observed, with H_2 as electron donor instead of formate when CO_2 was omitted. If CO_2 and ferredoxin were present simultaneously, both were reduced concurrently, although apparently without any coupling because the velocity of

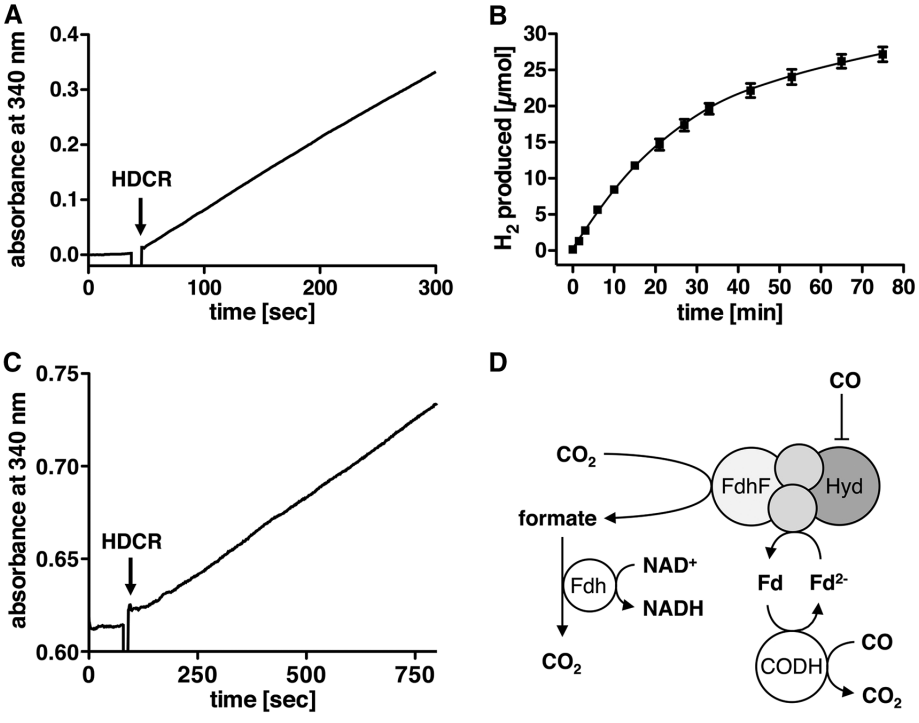

Fig. 1. Reactions catalyzed by the purified HDCR complex. (**A**) Formate production from H_2 + CO_2. At the time point indicated, 2 μg HDCR was added. Formate was measured using nicotinamide adenine dinucleotide (NAD)–dependent FDH from *Candida boidinii*. (**B**) Hydrogen production from formate (50 mM) (10 μg HDCR). All data points are mean ± SEM; N = 6 independent experiments. (**C**) Formate production with ferredoxin as electron donor (3.5 μg HDCR). (**D**) Set-up of the measurement from (C). Ferredoxin was reduced by CODH with electrons from CO oxidation. Formate was measured as described for (A).

each reaction did not vary in dependence with the other one.

Because the reduction of CO_2 does not require additional cellular electron carriers, the conversion is independent of the cell metabolism. This opens the possibility of using the HDCR in whole-cell catalysis by separating growth and energy conservation from the hydrogenation of CO_2. To test this, we used whole cells of *A. woodii* that produce acetate as the major end product from $H_2 + CO_2$. The energy metabolism of *A. woodii* is strictly sodium ion–dependent and depends on a sodium ion gradient across the cytoplasmic membrane (*15*). We used this trait to block the energy metabolism by omitting sodium ions from the buffer or by adding a sodium ionophore (fig. S9). Under these conditions, acetate production ceased almost completely, and formate was produced with an initial rate of 2 μmol min^{-1} mg^{-1} cell protein (fig. S10). The formate produced was excreted from the cells. Formate production from $H_2 + CO_2$ using whole cells was also observed in other systems, but different enzymes seem to be responsible there (*16*–*18*). For further experiments, we used $KHCO_3$ as substrate; thereby, the overall process is almost pH neutral compared with the production of formic acid from CO_2. The genome of *A. woodii* encodes for a carboanhydrase that allows the rapid interconversion of CO_2 and HCO_3^-. Up to 0.45 M HCO_3^-, the final formate concentration increased with increasing substrate concentration (Fig. 3). At 1×10^5 Pa H_2, the thermodynamic equilibrium is approximately $[HCO_3^-] = [HCOO^-]$. Indeed, up to 0.45 M HCO_3^- the final formate concentration fits well to the theoretic thermodynamic limit of the reaction, underlining the independence of the carboxylation of CO_2/HCO_3^- from other cellular processes. There is apparently no substantial loss in unwanted side products or biomass production.

Acetogenic bacteria such as *A. woodii* are also able to use syngas, a mixture of H_2, CO_2, and CO, as substrate for acetogenesis. Syngas fermentation is an increasingly considered "green" option for the production of chemicals (*19*). As a proof of principle, we tested whether syngas can also be used as substrate for the production of formate. Indeed, HDCR in combination with CODH catalyzed formate production from syngas with 1.3 U/mg (Fig. 4A). The whole cell system produced formate from syngas as well, albeit with lower activities compared with $H_2 + CO_2$ alone (Fig. 4B). In contrast to $H_2 + CO_2$ as substrate, acetate formation could not completely be inhibited in our test system. Based on the results with whole cells, a two-step process can be imagined where the bacteria could be grown using syngas or a mixture of only $H_2 + CO_2$ as a substrate, and by disabling the metabolism the hydrogenation of CO_2 could be induced and H_2 could be stored as formate (fig. S11). In this scenario, the greenhouse gas CO_2 is not only used as storage material for H_2 but, additionally, is consumed as growth substrate.

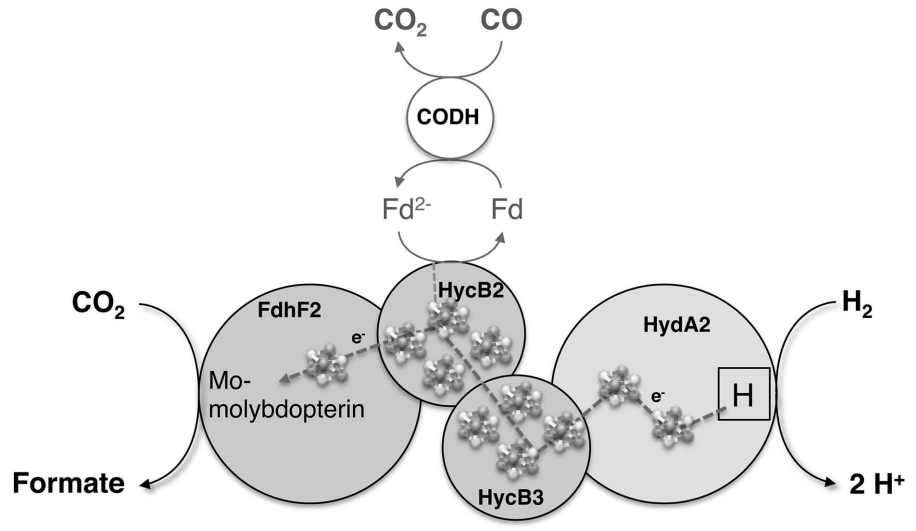

Fig. 2. Model of the HDCR from *A. woodii*. Electrons for CO_2 reduction are either provided by the hydrogenase subunit HydA2, where hydrogen oxidation takes place, or by reduced ferredoxin. The latter can be reduced using carbon monoxide and CODH, for example. Electrons are delivered to the active site for CO_2 reduction in FdhF2 via the electron-transferring subunits HycB2/3. Iron sulfur clusters are indicated.

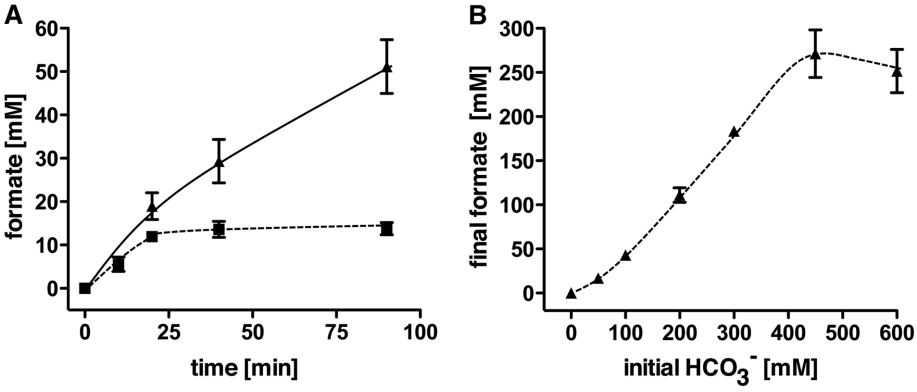

Fig. 3. Production of formate using whole-cell catalysis. (**A**) Whole cells of *A. woodii* were incubated with H_2 and CO_2 (squares) or H_2 and 0.3 M $KHCO_3$ in buffer containing 30 μM ETH2120 and 20 mM NaCl. (**B**) The final concentration of formate that was produced by whole cells is plotted against the initial concentration of HCO_3^- used (100% H_2 as gas phase). All data points are mean ± SEM; $N = 3$ independent experiments.

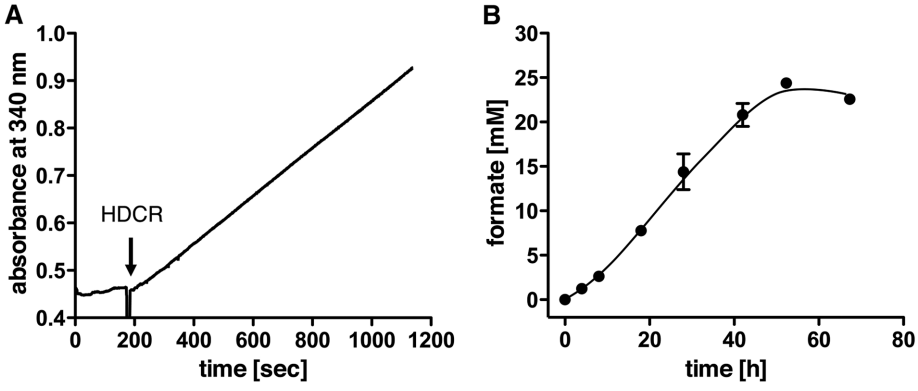

Fig. 4. Formate production from syngas. (**A**) Purified HDCR (4 μg) together with CODH and ferredoxin catalyzed formate production from syngas. Formate was measured using NAD-dependent FDH from *C. boidinii*. (**B**) Formate was also produced from syngas by whole cells in the presence of ETH2120 and NaCl. At the final time point, 60 mM acetate were produced in addition to formate. All data points are mean ± SEM; $N = 3$ independent experiments.

We finally want to address the physiological implications of the properties of HDCR. Based on the genome sequence, the two FDHs in the HDCR context seem to be the only enzymes with FDH activity in *A. woodii*. Thus, the HDCR complex is essential for the first step in the reductive acetyl-CoA pathway. In agreement with this notion are data from proteome analysis, which revealed no differential expression between H_2 + CO_2 or fructose as substrate (*13*). Acetogenesis from fructose or other substrates does not yield H_2 directly but reduced ferredoxin. Thus, the second H_2-independent entry path for electrons is favorable. In addition, CO inhibits the hydrogenase module, but CO-derived electrons can still enter the complex for CO_2 reduction via ferredoxin. The ferredoxin entry path also ensures growth at low H_2 partial pressures. Then the electron-bifurcating hydrogenase may generate reduced ferredoxin for CO_2 reduction (*20*).

Enzymes similar to the HDCR reported here seem to play an important role in other bacteria as well (see table S2 for the occurrence and previous description of HDCR-like gene clusters in other prokaryotic genomes). A similar gene cluster was predicted in the acetogen *Treponema primitia* (*21*). HDCR-type enzymes are not restricted to acetogens, but they, for example, have also proposed functions in sulfate reducing organisms (*22*) and syntrophic associations (*23*). Some gene clusters coding for predicted HDCRs vary in the composition compared with the enzyme in the present study—for example, the number of hydrogenase subunits.

References and Notes

1. L. Schlapbach, A. Züttel, *Nature* **414**, 353–358 (2001).
2. S. Enthaler, J. von Langermann, T. Schmidt, *Energy Environ. Sci.* **3**, 1207–1217 (2010).
3. N. M. Aslam, M. S. Masdar, S. K. Kamarudin, W. R. W. Daud, *APCBEE Procedia* **3**, 33–39 (2012).
4. E. Fujita, J. T. Muckerman, Y. Himeda, *Biochim. Biophys. Acta* **1827**, 1031–1038 (2013).
5. J. F. Hull *et al*., *Nat. Chem.* **4**, 383–388 (2012).
6. M. S. Jeletic, M. T. Mock, A. M. Appel, J. C. Linehan, *J. Am. Chem. Soc.* **135**, 11533–11536 (2013).
7. B. R. Crable, C. M. Plugge, M. J. McInerney, A. J. Stams, *Enzyme Res.* **2011**, 532536 (2011).
8. A. M. Appel *et al*., *Chem. Rev.* **113**, 6621–6658 (2013).
9. T. Reda, C. M. Plugge, N. J. Abram, J. Hirst, *Proc. Natl. Acad. Sci. U.S.A.* **105**, 10654–10658 (2008).
10. S. L. D. H. L. Drake, C. Matthies, K. Küsel, in *Acetogenesis,* H. L. Drake, Ed. (Chapman and Hall, New York, 1994), pp. 3–60.
11. V. Müller, F. Imkamp, A. Rauwolf, K. Küsel, H. L. Drake, in *Strict and Facultative Anaerobes: Medical and Environmental Aspects,* M. M. Nakano, P. Zuber, Eds. (Horizon Biosciences, Norfolk, 2004), pp. 251–281.
12. S. Wang *et al*., *J. Bacteriol.* **195**, 4373–4386 (2013).
13. A. Poehlein *et al*., *PLOS ONE* **7**, e33439 (2012).
14. Materials and methods are available as supplementary materials on *Science online*.
15. S. Schmidt, E. Biegel, V. Müller, *Biochim. Biophys. Acta* **1787**, 691–696 (2009).
16. S. M. da Silva *et al*., *Microbiology* **159**, 1760–1769 (2013).
17. W. M. Wu, R. F. Hickey, M. K. Jain, J. G. Zeikus, *Arch. Microbiol.* **159**, 57–65 (1993).
18. A. M. Klibanov, B. N. Alberti, S. E. Zale, *Biotechnol. Bioeng.* **24**, 25–36 (1982).
19. P. C. Munasinghe, S. K. Khanal, *Bioresour. Technol.* **101**, 5013–5022 (2010).
20. K. Schuchmann, V. Müller, *J. Biol. Chem.* **287**, 31165–31171 (2012).
21. E. G. Matson, X. Zhang, J. R. Leadbetter, *Environ. Microbiol. Rep.* **12**, 2245–2258 (2010).
22. I. A. Pereira *et al*., *Front. Microbiol.* **2**, 69 (2011).
23. N. Müller, P. Worm, B. Schink, A. J. Stams, C. M. Plugge, *Environ. Microbiol. Rep.* **2**, 489–499 (2010).

Acknowledgments: We are grateful to M. Herzberg and D. Nies for the ICP-MS measurements and to J. Langer for protein identification via peptide mass fingerprinting. This work was supported by grants from the Deutsche Forschungsgemeinschaft and the German National Academic Foundation. Part of this work is filed as a patent (EP-No. 13172411.4). The data reported in this paper are tabulated in the supplementary materials.

Supplementary Materials

www.sciencemag.org/content/342/6164/1382/suppl/DC1
Materials and Methods
Figs. S1 to S11
Tables S1 and S2
References (*24*–*28*)

15 August 2013; accepted 28 October 2013
10.1126/science.1244758

Genetic and Molecular Basis of Drug Resistance and Species-Specific Drug Action in Schistosome Parasites

Claudia L. L. Valentim,[1,2] Donato Cioli,[3] Frédéric D. Chevalier,[2] Xiaohang Cao,[1] Alexander B. Taylor,[1] Stephen P. Holloway,[1] Livia Pica-Mattoccia,[3] Alessandra Guidi,[3] Annalisa Basso,[3] Isheng J. Tsai,[4] Matthew Berriman,[4] Claudia Carvalho-Queiroz,[1] Marcio Almeida,[2] Hector Aguilar,[5] Doug E. Frantz,[5] P. John Hart,[1,6]† Philip T. LoVerde,[1]*† Timothy J. C. Anderson[2]*†

Oxamniquine resistance evolved in the human blood fluke (*Schistosoma mansoni*) in Brazil in the 1970s. We crossed parental parasites differing ~500-fold in drug response, determined drug sensitivity and marker segregation in clonally derived second-generation progeny, and identified a single quantitative trait locus (logarithm of odds = 31) on chromosome 6. A sulfotransferase was identified as the causative gene by using RNA interference knockdown and biochemical complementation assays, and we subsequently demonstrated independent origins of loss-of-function mutations in field-derived and laboratory-selected resistant parasites. These results demonstrate the utility of linkage mapping in a human helminth parasite, while crystallographic analyses of protein-drug interactions illuminate the mode of drug action and provide a framework for rational design of oxamniquine derivatives that kill both *S. mansoni* and *S. haematobium*, the two species responsible for >99% of schistosomiasis cases worldwide.

In the absence of effective vaccines for human helminth infections, repeated rounds of mass treatment with drug monotherapies are typically used for control in most developing countries (*1*, *2*). These programs bring enormous health benefits but impose strong selection on parasite populations, and resistance is suspected for several helminth species, including *Onchocerca volvulus*, cause of river blindness, and *Wuchereria bancrofti*, cause of lymphatic filariasis (*3*, *4*). However, resistance to oxamniquine (OXA) in *Schistosoma mansoni*, a trematode parasite that infects 67 million people in Africa and South America (*1*), provides the first and clearest example of naturally selected drug resistance in a human helminth parasite. OXA was the first-line drug in Brazil until the late 1990s and remained in use until 2010. Resistant parasites were isolated from Brazilian patients in the 1970s (*5*, *6*) and also selected in the laboratory from sensitive parasite lines (*7*). Resistance has a recessive basis and results in a ~500% reduction in drug sensitivity (*8*). Genetic complementation experiments demonstrate that the same gene determines resistance in both field and laboratory-selected parasites, although whether the same mutations are responsible is unknown (*9*). OXA is species-specific (*10*, *11*), killing *S. mansoni* (67 million cases) but not other schistosome species (*S. haematobium*, 119 million cases) in Africa or *S. japonicum* (1 million cases) in Asia (*1*).

We exploited the *S. mansoni* genome sequence (*12*, *13*) and genetic map (*14*) to identify genome region(s) that underlie OXA-resistance and to determine the basis for species-specific drug action. The complete life cycle of *S. mansoni* can be maintained in the laboratory, and clonal expansion of larval parasites within the snail host allows production of thousands of genetically identical

[1]Departments of Biochemistry and Pathology, University of Texas Health Science Center, San Antonio, TX 78229, USA. [2]Texas Biomedical Research Institute, San Antonio, TX 78245, USA. [3]Institute of Cell Biology and Neurobiology, CNR, Rome, Italy. [4]Wellcome Trust Sanger Institute, Wellcome Trust Genome Campus, Hinxton, UK. [5]Department of Chemistry, The University of Texas at San Antonio, San Antonio, TX 78249, USA. [6]Department of Veterans Affairs, South Texas Veterans Health Care System, San Antonio, TX 78229, USA.

*These authors contributed equally.
†Corresponding author. E-mail: tanderso@txbiomedgenetics.org (T.J.C.A.); loverde@uthscsa.edu (P.T.L.); pjhart@biochem.uthscsa.edu (P.J.H.)